Acknowledgment. We are very grateful to IBM New Zealand Ltd. for providing large amounts of computer time. P.S. is very indebted to the Alexander von Humboldt-Stiftung for a FEODOR-LYNEN scholarship and for financial support. Thanks are due to Michael Dolg for providing part of the basis sets and pseudopotentials and to the Auckland University Grants Committee for partial support of this project. We also thank Martin A. Bennett, Ralph Cooney, and Graham A. Bowmaker for their interest in this work and very helpful comments, Cliff Rickard for his help in preparing the X-ray data, and Laurie P. Aldridge for critically reading this paper.

Registry No. $[AsPh_4]Au(SCN)_2$, 128444-83-7; AuH_2^-, 128444-80-4; $Au(CH_3)_2^-$, 57444-56-1; $Au(CN)_2^-$, 14950-87-9; $Au(SCN)_2^-$, 16073-82-8; $Au(PH_3)_2^+$, 128470-26-8; AuF_2^-, 55031-54-4; $AuCl_2^-$, 21534-24-7; $AuBr_2^-$, 23000-74-0; AuI_2^-, 23000-72-8; AuSCN, 128444-78-0; $AuCH_3$, 128444-79-1; AuCN, 506-65-0; $AuPH_3$, 128444-81-5; $AuPH_3^+$, 128444-82-6.

Supplementary Material Available: A table of observed and calculated structure factors for $[AsPh_4]Au(SCN)_2$ (7 pages). Ordering information is given on any current masthead page.

Contribution from the Department of Chemistry, University of California, Berkeley, California 94720

M{hydrotris(3-phenylpyrazol-1-yl)borate}$_2$: Sterically Encumbered Iron(II) and Manganese(II) Complexes

David M. Eichhorn and William H. Armstrong*

Received August 28, 1989

The sterically congested complexes $M(tppb)_2$ (M = Fe, Mn; tppb = hydrotris(3-phenylpyrazol-1-yl)borate) were isolated in good yields from reaction mixtures containing 1 equiv of $M(CF_3SO_3)_2$ and 2 equiv of Ktppb. The iron complex $Fe(tppb)_2$ (**1**) crystallizes in the monoclinic space group $P2_1/n$ with a = 12.896 (3) Å, b = 19.547 (3) Å, c = 21.260 (8) Å, β = 94.03 (1)°, V = 5346 (4) Å^3, and Z = 4. The manganese analogue $Mn(tppb)_2$ (**2**) crystallizes in the orthorhombic space group *Ibca* with a = 19.664 (6) Å, b = 22.271 (8) Å, c = 23.680 (5) Å, V = 10371 (6) Å^3, and Z = 8. The M-N bond lengths in compounds **1** and **2**, particularly for **1**, are markedly longer than corresponding lengths for complexes of less sterically demanding poly(pyrazolyl)borate ligands. The magnetic properties of **1** and **2** are typical of S = 2 and $S = {}^5/_2$ species, respectively. The most dramatic difference between the properties of **1** and **2** and their less sterically hindered counterparts lies in their electrochemical behavior. For example, the Fe^{III}/Fe^{II} reduction potential for **1** is approximately 0.6 V more positive than for $Fe(HB(pz)_3)_2$ ($HB(pz)_3$ = hydrotris(pyrazol-1-yl)borate).

Introduction

The use of tris(pyrazolyl)borate ligands has become increasingly popular in synthetic inorganic, bioinorganic, and organometallic chemistry.[1a] As facially capping tridentate nitrogen donors, they have been used as a convenient substitute for cyclopentadienyl ligands, forming complexes which often demonstrate properties similar to their cyclopentadienyl counterparts.[1b] In bioinorganic chemistry, the tris(pyrazolyl)borates have been used as mimics for imidazole coordination in models for active sites of metalloenzymes.[2] One of the problems encountered in the use of tris(pyrazolyl)borates is their propensity to form ML_2 complexes with transition metals. In order to prevent or retard the formation of such complexes, tris(pyrazolyl)borate ligands with substitution at the 3- and 5-positions of the pyrazole rings have been employed.[3,4]

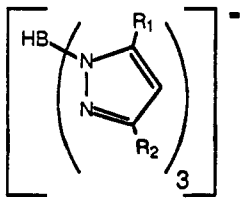

tppb : R_1 = H, R_2 = C_6H_5

The most commonly used of such ligands, hydrotris(3,5-dimethylpyrazol-1-yl)borate, will form ML_2 complexes, but not as readily as the unsubstituted ligand.[3a] Recent reports have described the synthesis and complex formation of the significantly more bulky ligand hydrotris(3-phenylpyrazol-1-yl)borate (tppb), which forms stable complexes of the type ML(SCN)(THF) (M = first-row transition elements), and it was postulated that this ligand would not allow ML_2 formation.[4] As part of our efforts toward modeling the active sites of non-heme iron-containing oxygenases, we were interested in using this ligand to prevent formation of ML_2 complexes. In marked contrast to previous results, we discovered that although formation of MLX complexes is possible, in the absence of strongly coordinating anions the ML_2 complex is formed preferentially. Even when a 1:1 ligand:metal ratio was employed, the ML_2 product was isolated. We report here the syntheses, structures, and properties of the remarkably sterically encumbered $M(tppb)_2$ (M = Fe, Mn) complexes.

Experimental Section

General Procedures. Unless otherwise stated, all materials were used as received without further purification. When dry, degassed solvents are specified, they were distilled from potassium/benzophenone ketyl (THF),[5] sodium (hexanes), or CaH_2 (CH_2Cl_2) and degassed by purging

(1) (a) Trofimenko, S. *Prog. Inorg. Chem.* **1986**, *34*, 115. (b) Trofimenko, S. *Inorg. Chem.* **1969**, *8*, 2675.
(2) (a) Armstrong, W. H.; Spool, A.; Papaefthymiou, G. C.; Frankel, R. B.; Lippard, S. J. *J. Am. Chem. Soc.* **1984**, *106*, 3653. (b) Thompson, J. S.; Marks, T. J.; Ibers, J. A. *J. Am. Chem. Soc.* **1979**, *101*, 4180.
(3) (a) Cleland, W. E.; Barnhart, K. M.; Yamanouchi, K.; Collison, D.; Mabbs, F. E.; Ortega, R. B.; Enemark, J. H. *Inorg. Chem.* **1987**, *26*, 1017. (b) Trofimenko, S.; Calabrese, J. C.; Domaille, P. J.; Thompson, J. S. *Inorg. Chem.* **1989**, *28*, 1091.
(4) Trofimenko, S.; Calabrese, J. C.; Thompson, J. S. *Inorg. Chem.* **1987**, *26*, 1507.
(5) Abbreviations used in this paper: THF, tetrahydrofuran; tppb, hydrotris(3-phenylpyrazol-1-yl)borate; $HB(Me_2pz)_3$, hydrotris(3,5-dimethylpyrazol-1-yl)borate; $HB(pz)_3$, hydrotris(pyrazol-1-yl)borate; tacn, 1,4,7-triazacyclononane; SSCE, saturated sodium calomel electrode; SCE, saturated calomel electrode; NHE, normal hydrogen electrode; TMS, tetramethylsilane; 2-Mephen, 2-methyl-1,10-phenanthroline; MeIm, *N*-methylimidazole; bpy, bipyridyl; terpy, terpyridine; bbt, 2-bis[(2-benzimidazolylmethyl)amino]ethanol; TPP, 5,10,15,20-tetraphenylporphyrinate; EDTA, ethylenediaminetetraacetate; [16]aneN$_5$, 1,4,7,10,13-pentaazacyclohexadecanate; ibz, *N*,*N*-bis(2-benzimidazolylmethyl)amine; $TPP(CN)_3$, 3,8,13-tricyano-5,10,15,20-tetraphenylporphyrinate; $(TPP)Br_4$, 3,8,13,18-tetrabromo-5,10,15,20-tetraphenylporphyrinate $TPP(CN)_4$, 3,8,13,18-tetracyano-5,10,15,20-tetraphenylporphyrinate; dtne, 1,2-bis(1,4,7-triaza-1-cyclononyl)ethane; Fc, ferrocene; phen, 1,10-phenanthroline; Mesaldpt, 1,9-bis(2-hydroxybenzylidene)-1,5,9-triazanonanate; Pctad, bis(2-pyrrolidylidene)-1,5,8,12-tetraazadodecanate; Saltad, 1,12-bis(2-hydroxybenzylidene)-1,4,9,12-tetraazadodec-6-enate; py-pentaamine, 3,6,10,13,19-pentaazabicyclo[13.3.1]nonadeca-1(19),15,17-triene; PhIO, iodosobenzene; MCPBA, *m*-chloroperoxybenzoic acid.

0020-1669/90/1329-3607$02.50/0

with nitrogen before use. Manipulations of air-sensitive compounds were performed under a nitrogen atmosphere in a Vacuum Atmospheres glovebox, Type Dry Lab HE-43-2, equipped with a Vacuum Atmospheres purification Dry Train Mo40-1 and on a double-manifold Schlenk line by using standard Schlenk techniques. ^{1}H NMR spectra were taken on a 250-MHz Fourier transform spectrometer, constructed in the UC Berkeley NMR laboratory by Rudi Nunlist, equipped with a Cryomagnets, Inc., magnet and a Nicolet Model 1280 data collection system. ^{13}C NMR spectra were taken on a Bruker AM-400 spectrometer. IR spectra were recorded on a Nicolet 5DX Fourier transform infrared spectrometer. Solid-state magnetic susceptibility measurements were performed on a Johnson-Matthey Model MSB-1 magnetic balance. Elemental analyses were performed by the UC Berkeley Microanalytical Laboratory (C, H, N) and Galbraith Laboratories, Inc., Knoxville, TN (Fe, Mn). EPR spectra were taken on an IBM ER 2090D-SRC spectrometer. Electrochemistry was performed with an EG&G Princeton Applied Research Model 264A polarographic analyzer/stripping voltammeter equipped with a locally constructed Supercycle triangle wave generator[6] and using a platinum-disk working electrode, a saturated sodium calomel reference electrode, and a platinum-wire auxiliary electrode.

Preparation of Compounds. Potassium Hydrotris(3-phenylpyrazol-1-yl)borate (Ktppb). In a modification of the procedure described by Trofimenko et al.,[4] 5.60 g (38.8 mmol) of 3-phenylpyrazole and 640 mg (11.9 mmol) of KBH_4 were placed in a flask with 20 mL of anhydrous anisole. As the mixture was slowly heated with an oil bath, the pyrazole dissolved, creating a yellow solution. The temperature was slowly increased until reflux was achieved. The solution was heated at reflux until hydrogen gas evolution had ceased and the white product had precipitated (approximately 2 days). The product was collected by filtration and washed with hexanes and hot toluene. Purification was achieved by stirring with Celite in THF, filtering, and removing the solvent. This procedure afforded a combined yield of 4.83 g (85%) of white powder. IR (KBr pellet, cm^{-1}): 697 (s, phenyl C–H), 750 (vs, phenyl C–H), 1044 (s), 1073 (s), 1099 (s), 1191 (vs), 1245 (m), 1349 (m), 1459 (s), 2411 (w, B–H). ^{1}H NMR (DMSO, δ downfield of TMS): 6.50 (d, 1 H), 7.21 (t, 2 H), 7.33 (t, 2 H), 7.49 (d, 1 H), 7.77 (d, 2 H). ^{13}C NMR (DMSO, δ downfield of TMS): 100.83, 124.94, 126.31, 128.39, 134.65, 135.29, 150.34. Anal. Calcd for $C_{27}H_{22}N_6KB$: C, 67.50; H, 4.62; N, 17.49. Found: C, 67.31; H, 4.76; N, 17.24.

Metal Complexes. Fe(tppb)$_2$ (1). Preparation of the iron(II) complex was carried out under nitrogen with dry, deoxygenated solvents. To solid $Fe(CF_3SO_3)_2$ (540 mg, 1.52 mmol) was added a solution of 1.466 g (3.05 mmol) of Ktppb in 50 mL of THF. The solution was stirred for 2 h, and the solvent was removed in vacuo. The resulting white powder was dissolved in 50 mL of CH_2Cl_2, and 50 mL of hexanes was added. Cooling at −14 °C yielded 780 mg of colorless crystals, which were collected by filtration. Solvent was removed from the filtrate, and the remaining white solid was recrystallized from CH_2Cl_2/hexanes to yield a second crop of 320 mg of colorless crystals, giving a total yield of 1.100 g (77%) of **1**. IR (KBr pellet, cm^{-1}): 676 (m), 691 (s, phenyl C–H), 739 (m), 753 (vs, phenyl C–H), 784 (w), 1049 (s), 1058 (s), 1073 (m), 1127 (m), 1189 (s), 1254 (w), 1275 (w), 1341 (w), 1370 (s), 1465 (s), 1498 (s), 1520 (w), 2471 (w, B–H), 3029 (w), 3061 (w). ^{1}H NMR ($CDCl_3$, δ downfield of TMS): −14.20, −7.84, −3.89, 0.88, 1.27, 3.76, 5.32, 7.53, 9.14, 12.2, 27.8, 43.3, 48.1, 50.4. Solid-state magnetic susceptibility (Faraday method): μ_{eff} = 5.10 μ_B. Solution magnetic susceptibility (Evans method):[7] μ_{eff} = 5.07 μ_B. Anal. Calcd for $C_{54}H_{44}N_{12}B_2Fe$ (Fe(tppb)$_2$): C, 69.11; H, 4.73; N, 17.91; Fe, 5.95. Found: C, 68.91; H, 4.71; N, 17.54; Fe, 5.72. Electrochemistry (CH_2Cl_2, NBu_4PF_6): $E_{1/2}$(vs SSCE) = 0.855 V, $E_{p,a} - E_{p,c}$ = 0.254 V, i_a/i_c = 0.96.

Mn(tppb)$_2$ (2). To solid $Mn(CF_3SO_3)_2$·2MeCN (540 mg, 1.24 mmol) was added a solution of 1.192 g (2.48 mmol) of Ktppb in 50 mL of THF. The solution was stirred for 2 h, and the solvent was removed under vacuum. The resulting white powder was dissolved in 50 mL of CH_2Cl_2, and 50 mL of hexanes was added. Cooling this solution at −14 °C yielded 510 mg of colorless crystals, which were collected by filtration. Solvent was removed from the filtrate, and the remaining white solid was recrystallized two more times from CH_2Cl_2/hexanes to afford crops of 190 and 130 mg of colorless crystals, giving a total yield of 830 mg (71%) of **2**. IR (KBr pellet, cm^{-1}): 676 (m), 693 (s, phenyl C–H), 739 (m), 753 (vs, phenyl C–H), 783 (w), 996 (w), 1029 (m), 1048 (s), 1075 (m), 1127 (m), 1188 (s), 1198 (s), 1253 (w), 1278 (w), 1346 (w), 1368 (s), 1464 (s), 1497 (s), 1521 (w), 2467 (w, B–H), 3031 (w), 3058 (w). Solid-state magnetic susceptibility (Faraday method): μ_{eff} = 6.06 μ_B. Anal. Calcd for Mn(tppb)$_2$·1.4CH_2Cl_2: C, 62.98; H, 4.51; N, 15.91; Mn, 5.20. Found: C, 63.39; H, 4.51; N, 16.20; Mn, 6.08. Electrochemistry (CH_2Cl_2, NBu_4PF_6): E(vs SSCE) = 1.68 V (irreversible), −1.66 V (irreversible). EPR (298 K, CH_2Cl_2): six-line pattern, g = 1.99, A = 8.30 × 10^{-3} cm^{-1}.

Table I. Crystallographic Data for Fe(tppb)$_2$ (**1**) and Mn(tppb)$_2$ (**2**)[a]

	1	2
formula	$C_{54}H_{44}N_{12}B_2Fe$[b]	$C_{54}H_{44}N_{12}B_2Mn$[b]
t, °C	−110	−143
cryst syst	monoclinic	orthorhombic
space group	$P2_1/n$	$Ibca$
a, Å	12.896 (3)	19.664 (6)
b, Å	19.547 (3)	22.271 (8)
c, Å	21.260 (8)	23.680 (5)
β, deg	94.03 (1)	90
V, Å^3	5346 (4)	10371 (6)
Z	4	8
d_{calc}, g/cm^3	1.36	1.35
d_{obsd}, g/cm^3	1.33	1.32
μ, cm^{-1}	4.33	4.10
diffractometer	CAD4	$P2_1$
λ(Mo Kα), Å	0.71073	0.71073
monochromator	graphite	graphite
cryst size, mm	0.24 × 0.28 × 0.28	0.42 × 0.47 × 0.50
octants collcd	$h,k,\pm l$	hkl (for $h + k + l = 2n$)
max hkl	13,21,22	23,26,28
2θ range, deg	2–45	0–50
collcn method	θ–2θ	ω
no of data collcd	7761	4902
no. of data used ($I > 3\sigma(I)$)	5785	2969
no. of variables	702	340
R	0.0500	0.0493
R_w	0.0360	0.0657
largest peak on final diff Fourier map, e/Å^3	0.45	0.79
gof	2.34	1.44

[a] Formulas used in structure solution: $R = (\sum||F_o| - |F_c||)/\sum|F_o|$; $R_w = \{[\sum w(|F_o| - |F_c|)^2]/\sum wF_o^2\}^{1/2}$; gof = $\{[\sum w(|F_o| - |F_c|)^2]/(n_o - n_v)\}^{1/2}$. Function minimized: $\sum w(|F_o| - |F_c|)^2$; $w = 1/\sigma^2(F_o)$ (Fe(tppb)$_2$); $w = 1/(\sigma^2(F) + 0.001F^2)$ (Mn(tppb)$_2$). [b] The molecular formulas represent the metal complexes only. The actual species present in the crystals are **1**·CH_2Cl_2·C_6H_{12} (fw = 1022.65) and **2**·1.4CH_2Cl_2 (fw = 1057.90).

X-ray Data Collection and Structure Solutions. Fe(tppb)$_2$. Colorless trapezoidal crystals suitable for X-ray diffraction studies were grown by dissolving in CH_2Cl_2, adding an equal volume of hexanes, and cooling to −35 °C. Due to a propensity for solvent loss, the crystal was affixed to a glass fiber under a stream of cold nitrogen by silicon grease and immediately transferred to the cold stream of the diffractometer. Cell parameters were determined by using 25 reflections with 8.3° < θ < 12.3°.

The iron atom position was determined by interpretation of the Patterson map, and the structure was refined by standard full-matrix least-squares and Fourier techniques with a Digital Equipment Micro-Vax computer using locally modified Nonius SDP[8] software. No absorption correction was applied to the data. Non-hydrogen atoms were refined anisotropically. Hydrogen atoms were located on a difference Fourier map, and they were included in structure factor calculations at idealized positions, but were not refined. A disordered hexane molecule was modeled by isotropic carbon atoms with varying multiplicities. Further details are given in Table I.

Mn(tppb)$_2$. Colorless X-ray-quality crystals were grown in the same manner as for the Fe complex. The crystal was affixed to a glass fiber with oil and transferred to the cold stream of the diffractometer.

The manganese atom position was determined by using the SHELXS[9] Patterson interpretation program, and the structure was refined by least-squares and Fourier techniques using SHELX[10] software on a Digital Equipment Micro-Vax computer. An absorption correction was not

(6) Woodward, W. S.; Rocklin, R. D.; Murray, R. W. *Chem. Biomed. Environ. Instrum.* **1979**, *9*, 95.
(7) (a) Evans, D. F. *J. Chem. Soc.* **1959**, 2003. (b) Klein, M. P.; Holder, B. E. *Phys. Rev.* **1955**, *98*, 265.
(8) Frenz, B. A. *Structure Determination Package*; Texas A&M University and Enraf-Nonius: College Station, TX, and The Netherlands, 1985 (as revised locally by Dr. Frederick J. Hollander).
(9) Sheldrick, G. SHELXS-86.
(10) Sheldrick, G. SHELX-76: A Program for Crystal Structure Determination, 1976.
(11) Oliver, J. D.; Mullica, D. F.; Hutchinson, B. B.; Milligan, W. O. *Inorg. Chem.* **1980**, *19*, 165.

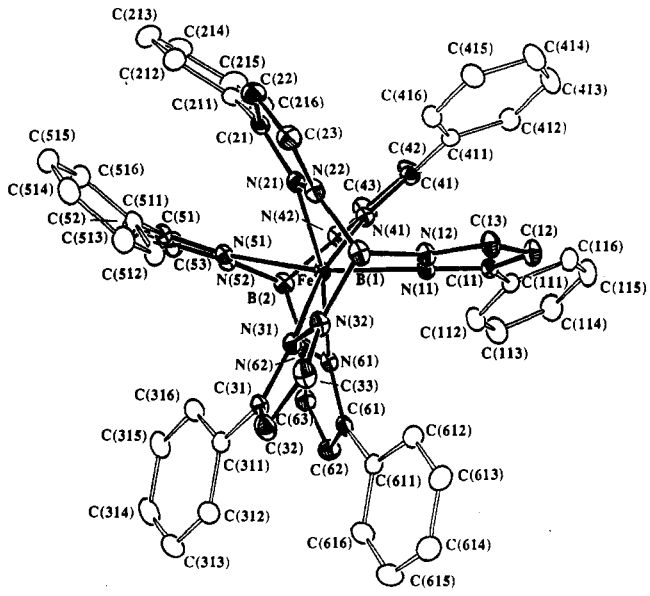

Figure 1. Crystal structure of $Fe(tppb)_2$ (**1**) showing the atom-labeling scheme. Hydrogen atoms are omitted for clarity.

applied to the data. Non-hydrogen atoms were refined anisotropically, except for the partially occupied CH_2Cl_2 carbon atoms, which were refined isotropically. The disordered CH_2Cl_2 molecule was modeled by adjusting the multiplicities of the atoms to give the best *R* factor and reasonable thermal parameters. Hydrogen atoms were located on a difference Fourier map, and they were included in structure factor calculations at idealized positions, but were not refined. Further details are given in Table I.

Synthesis of Compounds

The synthesis of the ligand was accomplished in a straightforward manner based on the literature procedure.[4] It was discovered that initial preparation and isolation of the dihydrobis(3-phenylpyrazol-1-yl)borate was not necessary. In fact, addition of all 3 equiv of the pyrazole in the beginning of the preparation followed by refluxing in anisole for 2 days gave a considerably higher yield than previously reported.

The metal complexes were synthesized by adding a THF solution of the ligand (as the potassium salt) to the triflate salt of the metal. The initial intent was to form a complex containing only one ligand molecule per iron, and the reaction mixture accordingly contained equimolar amounts of ligand and metal. The absence of infrared bands corresponding to triflate vibrations in the products which contained tppb indicated that the only species formed was the ML_2 complex, so the preparation was repeated by using a 2:1 ligand:metal ratio. In order to confirm that an MLX complex can be made with iron, a similar reaction was carried out with a THF solution of the ligand added to $Fe(CF_3SO_3)_2$ and KSCN in a 1:1:1 ratio. This resulted in isolation of Fe(tppb)(SCN)(THF),[12] which has a structure analogous to the previously reported Co complex.[4]

Synthesis of the $M(tppb)_2$ complexes can easily be monitored by infrared spectroscopy. The B–H stretch, which occurs at 2411 cm^{-1} in Ktppb, shifts to higher energy in the metal complexes (2471 cm^{-1} for Fe and 2467 cm^{-1} for Mn). This behavior is analogous to that seen upon formation of one-to-one metal complexes of tppb.[4] The presence of unreacted $Fe(CF_3SO_3)_2$ can be detected by the triflate vibrations at 636, 575, and 520 cm^{-1} in the IR spectrum.

Table II. Atomic Coordinates and Isotropic Thermal Parameters for $Fe(tppb)_2$ (**1**)

atom	*x*	*y*	*z*	B_{eqv}, Å^{2a}
Fe	0.08166 (3)	0.25157 (2)	0.08460 (2)	1.526 (8)
N(11)	−0.0621 (2)	0.1986 (1)	0.0409 (1)	1.71 (5)
N(12)	−0.0611 (2)	0.1309 (1)	0.0582 (1)	1.90 (5)
N(21)	0.1740 (2)	0.1581 (1)	0.0648 (1)	1.83 (5)
N(22)	0.1265 (2)	0.1003 (1)	0.0854 (1)	1.98 (5)
N(31)	0.0450 (2)	0.2076 (1)	0.1779 (1)	1.70 (5)
N(32)	0.0134 (2)	0.1407 (1)	0.1706 (1)	1.91 (5)
N(41)	0.0895 (2)	0.3026 (1)	−0.0093 (1)	1.73 (5)
N(42)	0.1231 (2)	0.3688 (1)	−0.0021 (1)	2.04 (5)
N(51)	0.2388 (2)	0.2936 (1)	0.1161 (1)	1.68 (5)
N(52)	0.2485 (2)	0.3592 (1)	0.0947 (1)	1.88 (5)
N(61)	0.0105 (2)	0.3481 (1)	0.1196 (1)	1.73 (5)
N(62)	0.0665 (2)	0.4041 (1)	0.1039 (1)	1.92 (5)
C(11)	−0.1436 (2)	0.2057 (2)	−0.0025 (1)	1.77 (6)
C(12)	−0.1932 (2)	0.1422 (2)	−0.0127 (2)	2.38 (7)
C(13)	−0.1388 (2)	0.0969 (2)	0.0262 (2)	2.32 (7)
C(21)	0.2678 (2)	0.1376 (2)	0.0467 (1)	2.02 (6)
C(22)	0.2789 (3)	0.0671 (2)	0.0567 (2)	2.69 (7)
C(23)	0.1889 (3)	0.0459 (2)	0.0806 (2)	2.58 (7)
C(31)	0.0348 (2)	0.2230 (2)	0.2393 (1)	1.89 (6)
C(32)	−0.0036 (3)	0.1663 (2)	0.2703 (1)	2.63 (7)
C(33)	−0.0161 (3)	0.1162 (2)	0.2255 (1)	2.62 (7)
C(41)	0.0668 (2)	0.2941 (2)	−0.0722 (1)	1.99 (6)
C(42)	0.0849 (3)	0.3551 (2)	−0.1038 (1)	2.77 (7)
C(43)	0.1202 (3)	0.4004 (2)	−0.0580 (2)	2.86 (7)
C(51)	0.3334 (2)	0.2764 (2)	0.1435 (1)	1.85 (6)
C(52)	0.4025 (2)	0.3307 (2)	0.1384 (2)	2.73 (7)
C(53)	0.3463 (2)	0.3815 (2)	0.1079 (2)	2.77 (7)
C(61)	−0.0656 (2)	0.3727 (2)	0.1546 (1)	1.96 (6)
C(62)	−0.0564 (3)	0.4438 (2)	0.1605 (2)	2.64 (7)
C(63)	0.0275 (2)	0.4615 (2)	0.1278 (2)	2.44 (7)
C(111)	−0.1770 (2)	0.2704 (2)	−0.0325 (1)	1.76 (6)
C(112)	−0.1531 (2)	0.3334 (2)	−0.0051 (1)	2.43 (7)
C(113)	−0.1859 (3)	0.3937 (2)	−0.0345 (2)	3.04 (8)
C(114)	−0.2443 (3)	0.3917 (2)	−0.0918 (2)	3.08 (8)
C(115)	−0.2689 (3)	0.3296 (2)	−0.1189 (2)	2.82 (7)
C(116)	−0.2361 (2)	0.2691 (2)	−0.0900 (1)	2.28 (7)
C(211)	0.3464 (2)	0.1829 (2)	0.0210 (1)	2.22 (7)
C(212)	0.4511 (3)	0.1672 (2)	0.0328 (2)	2.97 (7)
C(213)	0.5270 (3)	0.2097 (2)	0.0116 (2)	3.78 (9)
C(214)	0.5002 (3)	0.2680 (2)	−0.0221 (2)	3.87 (9)
C(215)	0.3967 (3)	0.2830 (2)	−0.0360 (2)	3.52 (8)
C(216)	0.3203 (2)	0.2408 (2)	−0.0148 (2)	2.77 (7)
C(311)	0.0652 (2)	0.2883 (2)	0.2703 (1)	1.93 (6)
C(312)	0.0205 (2)	0.3060 (2)	0.3259 (1)	2.66 (7)
C(313)	0.0493 (3)	0.3658 (2)	0.3576 (2)	3.20 (8)
C(314)	0.1216 (3)	0.4093 (2)	0.3341 (2)	3.30 (8)
C(315)	0.1674 (3)	0.3918 (2)	0.2795 (2)	2.89 (7)
C(316)	0.1403 (2)	0.3313 (2)	0.2485 (1)	2.35 (7)
C(411)	0.0335 (2)	0.2293 (2)	−0.1029 (1)	1.83 (6)
C(412)	−0.0283 (2)	0.2311 (2)	−0.1593 (1)	2.44 (7)
C(413)	−0.0585 (3)	0.1716 (2)	−0.1898 (2)	2.94 (7)
C(414)	−0.0283 (3)	0.1086 (2)	−0.1653 (2)	2.97 (7)
C(415)	0.0336 (3)	0.1063 (2)	−0.1095 (2)	2.66 (7)
C(416)	0.0643 (2)	0.1661 (2)	−0.0786 (1)	2.16 (6)
C(511)	0.3595 (2)	0.2106 (2)	0.1748 (1)	1.85 (6)
C(512)	0.2872 (2)	0.1698 (2)	0.2026 (1)	2.37 (7)
C(513)	0.3157 (3)	0.1083 (2)	0.2309 (2)	2.65 (7)
C(514)	0.4183 (3)	0.0863 (2)	0.2330 (2)	2.88 (7)
C(515)	0.4917 (3)	0.1272 (2)	0.2070 (2)	2.91 (7)
C(516)	0.4632 (2)	0.1888 (2)	0.1783 (1)	2.50 (7)
C(611)	−0.1459 (2)	0.3301 (2)	0.1824 (1)	2.12 (6)
C(612)	−0.1805 (2)	0.2682 (2)	0.1574 (2)	2.48 (7)
C(613)	−0.2549 (3)	0.2306 (2)	0.1865 (2)	3.27 (8)
C(614)	−0.2964 (3)	0.2551 (2)	0.2399 (2)	3.66 (8)
C(615)	−0.2643 (3)	0.3173 (2)	0.2644 (2)	4.00 (9)
C(616)	−0.1901 (3)	0.3547 (2)	0.2361 (2)	3.10 (7)
B(1)	0.0167 (3)	0.1011 (2)	0.1089 (2)	2.08 (7)
B(2)	0.1587 (3)	0.3998 (2)	0.0622 (2)	2.03 (7)

[a] The thermal parameter given for anisotropically refined atoms is the isotropic equivalent thermal parameter defined as $(4/3)[a^2B(1,1) + b^2B(2,2) + c^2B(3,3) + ab(\cos\gamma)B(1,2) + ac(\cos\beta)B(1,3) + bc(\cos\alpha)B(2,3)]$ where *a*, *b*, and *c* are real cell parameters and $B(i,j)$ are anisotropic β.

(12) Eichhorn, D. M.; Armstrong, W. H. To be submitted for publication.
(13) Doedens, R. J.; Dahl, L. F. *J. Am. Chem. Soc.* **1966**, *88*, 4847.
(14) Goodwin, H. A.; Kucharski, E. S.; White, A. H. *Aust. J. Chem.* **1984**, *36*, 1115.
(15) Seel, F.; Lehnert, R.; Bill, E.; Trautwein, A. *Z. Naturforsch.* **1980**, *B35*, 631.
(16) Boeyens, J. C. A.; Forbes, A. G. S.; Hancock, R. D.; Weighardt, K. *Inorg. Chem.* **1985**, *24*, 2926.
(17) Kucharski, E. S.; McWhinnie, W. R.; White, A. H. *Aust. J. Chem.* **1978**, *31*, 53.
(18) Weiss, H.; Strahle, J. *Z. Naturforsch.* **1984**, *B39*, 1453.
(19) Baker, A. T.; Goodwin, H. A. *Aust. J. Chem.* **1985**, *38*, 207.

Table III. Atomic Coordinates and Isotropic Thermal Parameters for $Mn(tpp)_2$ (**2**)

atom	x	y	z	U_{eqv}, Å^{2a}
Mn	0.5000	0.2500	0.6626	0.0164
N(11)	0.4002 (2)	0.3040 (1)	0.6539 (1)	0.0184
N(12)	0.3446 (2)	0.2666 (1)	0.6514 (1)	0.0213
N(21)	0.4532 (2)	0.1817 (1)	0.5991 (1)	0.0218
N(22)	0.3885 (2)	0.1666 (1)	0.6150 (1)	0.0242
N(31)	0.4460 (2)	0.1969 (1)	0.7334 (1)	0.0179
N(32)	0.3791 (1)	0.1854 (1)	0.7201 (1)	0.0189
C(11)	0.3757 (2)	0.3607 (2)	0.6474 (1)	0.0202
C(111)	0.4179 (2)	0.4151 (2)	0.6478 (2)	0.0233
C(112)	0.4793 (2)	0.4193 (2)	0.6762 (2)	0.0255
C(113)	0.5166 (2)	0.4715 (2)	0.6764 (2)	0.0326
C(114)	0.4936 (3)	0.5213 (2)	0.6474 (2)	0.0457
C(115)	0.4320 (3)	0.5186 (2)	0.6194 (2)	0.0459
C(116)	0.3946 (2)	0.4661 (2)	0.6192 (2)	0.0338
C(12)	0.3050 (2)	0.3588 (2)	0.6413 (2)	0.0274
C(13)	0.2882 (2)	0.2988 (2)	0.6444 (2)	0.0274
C(21)	0.4698 (2)	0.1432 (2)	0.5566 (2)	0.0236
C(211)	0.5350 (2)	0.1442 (2)	0.5258 (2)	0.0249
C(212)	0.5559 (2)	0.0927 (2)	0.4970 (2)	0.0356
C(213)	0.6176 (2)	0.0917 (2)	0.4684 (2)	0.0427
C(214)	0.6586 (2)	0.1408 (2)	0.4680 (2)	0.0414
C(215)	0.6378 (2)	0.1927 (2)	0.4949 (2)	0.0316
C(216)	0.5766 (2)	0.1944 (2)	0.5233 (2)	0.0247
C(22)	0.4153 (2)	0.1045 (2)	0.5471 (2)	0.0404
C(23)	0.3658 (2)	0.1202 (2)	0.5845 (2)	0.0382
C(31)	0.4538 (2)	0.1781 (2)	0.7876 (2)	0.0210
C(311)	0.5193 (2)	0.1793 (2)	0.8185 (1)	0.0192
C(312)	0.5815 (2)	0.1762 (2)	0.7908 (2)	0.0235
C(313)	0.6420 (2)	0.1768 (2)	0.8208 (2)	0.0306
C(314)	0.6409 (2)	0.1797 (2)	0.8788 (2)	0.0294
C(315)	0.5794 (2)	0.1817 (2)	0.9072 (2)	0.0261
C(316)	0.5194 (2)	0.1814 (2)	0.8775 (2)	0.0214
C(32)	0.3920 (2)	0.1556 (2)	0.8079 (2)	0.0283
C(33)	0.3471 (2)	0.1609 (2)	0.7645 (2)	0.0285
B	0.3475 (2)	0.1985 (2)	0.6615 (2)	0.0226

[a] The isotropic equivalent thermal parameter for anisotropically refined atoms is defined as $[U(1,1) + U(2,2) + U(3,3) + (\cos\gamma)U(1,2) + (\cos\beta)U(1,3) + (\cos\alpha)U(2,3)]/3$.

Table IV. Selected Intramolecular Bond Lengths (Å) for $Fe(tppb)_2$ (**1**) and $Mn(tppb)_2$ (**2**)

1		**2**	
Fe–N(11)	2.265 (2)	Mn–N(11)	2.310 (3)
Fe–N(21)	2.237 (2)	Mn–N(21)	2.329 (3)
Fe–N(31)	2.242 (2)	Mn–N(31)	2.310 (3)
Fe–N(41)	2.240 (2)		
Fe–N(51)	2.244 (2)		
Fe–N(61)	2.248 (2)		
N(11)–N(12)	1.373 (3)	N(11)–N(12)	1.376 (4)
N(21)–N(22)	1.370 (3)	N(21)–N(22)	1.371 (4)
N(31)–N(32)	1.375 (3)	N(31)–N(32)	1.378 (4)
N(41)–N(42)	1.371 (3)		
N(51)–N(52)	1.369 (3)		
N(61)–N(62)	1.366 (3)		
N(12)–B(1)	1.533 (4)	N(12)–B	1.536 (6)
N(22)–B(1)	1.534 (4)	N(22)–B	1.531 (5)
N(32)–B(1)	1.528 (4)	N(32)–B	1.538 (5)
N(42)–B(2)	1.535 (4)		
N(52)–B(2)	1.528 (4)		
N(62)–B(2)	1.534 (4)		

The synthesis and crystallization of the iron complex were carried out under an inert atmosphere, due to the moderate air sensitivity of $Fe(tppb)_2$, solutions of which gradually turn brown in the air. However, once isolated in solid form, both the Mn(II) and Fe(II) species show no apparent signs of air oxidation for long periods of time.

Description of Structures

The structure of $Fe(tppb)_2$ (**1**) and atom-labeling scheme are shown in Figure 1. The asymmetric unit consists of the neutral complex, one CH_2Cl_2 molecule, and a disordered hexane molecule of crystallization. Each tppb ligand caps one face of an essentially octahedral coordination sphere. The iron atom resides on a general position in the monoclinic space group $P2_1/c$, but the complex displays nearly D_{3d} symmetry. In order for the two bulky tppb ligands to fit around the iron atom, they are coordinated with the phenyl rings on one ligand stacked with respect to those on the other ligand. Dihedral angles between neighboring phenyl substituents range from 2 to 10°. The phenyl rings are also twisted with respect to the pyrazole rings to which they are attached, with dihedral angles ranging from 23 to 31°. Of particular interest are the iron–nitrogen bond lengths, which range from 2.237 (2) to 2.265 (2) Å. These are considerably longer than the corresponding bond lengths for $Fe[HB(pz)_3]_2$,[11] $Fe[HB(3,5\text{-}Me_2pz)_3]_2$,[11] and Fe(tppb)(SCN)(THF)[12] (see Table VI). In order to accommodate these larger bond lengths, the pyrazole groups are spread further apart, with an average N–B–N angle of 110.9° compared with 107.5° in $Fe[HB(pz)_3]_2$,[11] 109.9° in $Fe[HB(3,5\text{-}Me_2pz)_3]_2$,[11] and 109.4° in Fe(tppb)(SCN)(THF).[4] Apparently, the steric demands of the ligand force the nitrogen atoms further away from the iron in order to form the ML_2 complex. These Fe–N bond distances are among the longest observed for iron–nitrogen species, the average Fe(II)–N bond length in crystallographically characterized complexes (excluding anomalously short Fe–NO and Fe–diazene bonds) being 2.05 Å,[20] with values ranging from 1.778 Å for tris(isonitrosomalonamido)ferrate(II)[21] to 2.511 Å for a complex of an N-substituted porphyrin[22] and 2.756 Å for

Table V. Selected Intramolecular Angles (deg) for $Fe(tppb)_2$ (**1**) and $Mn(tppb)_2$ (**2**)

1		**2**	
N(11)–Fe–N(21)	88.87 (8)	N(11)–Mn–N(21)	86.9 (1)
N(11)–Fe–N(31)	88.28 (8)	N(11)–Mn–N(31)	86.7 (1)
N(11)–Fe–N(41)	85.72 (8)	N(21)–Mn–N(31)	87.3 (1)
N(11)–Fe–N(51)	170.18 (9)		
N(11)–Fe–N(61)	100.29 (8)		
N(21)–Fe–N(31)	90.09 (8)		
N(21)–Fe–N(41)	97.94 (8)		
N(21)–Fe–N(51)	82.74 (8)		
N(21)–Fe–N(61)	169.42 (8)		
N(31)–Fe–N(41)	169.87 (8)		
N(31)–Fe–N(51)	96.80 (8)		
N(31)–Fe–N(61)	84.96 (8)		
N(41)–Fe–N(51)	90.37 (8)		
N(41)–Fe–N(61)	88.09 (8)		
N(51)–Fe–N(61)	88.56 (8)		
Fe–N(11)–N(12)	109.82 (16)	Mn–N(11)–N(12)	111.3 (2)
Fe–N(21)–N(22)	110.91 (17)	Mn–N(21)–N(22)	110.3 (2)
Fe–N(31)–N(32)	110.12 (16)	Mn–N(31)–N(32)	111.5 (2)
Fe–N(41)–N(42)	110.81 (16)		
Fe–N(51)–N(52)	110.23 (15)		
Fe–N(61)–N(62)	110.86 (17)		
Fe–N(11)–C(11)	143.56 (19)	Mn–N(11)–C(11)	142.7 (3)
Fe–N(21)–C(21)	142.39 (20)	Mn–N(21)–C(21)	142.6 (3)
Fe–N(31)–C(31)	143.89 (20)	Mn–N(31)–C(31)	142.3 (2)
Fe–N(41)–C(41)	143.36 (19)		
Fe–N(51)–C(51)	143.41 (19)		
Fe–N(61)–C(61)	143.58 (19)		

Table VI. Comparison of Fe–N Distances in Fe(II)–N_6 Complexes

complex	av Fe–N dist, Å	ref
$Fe(pyridine)_6^{2+}$	2.257	13
$Fe(tppb)_2$ (**1**)	2.246	this work
$Fe(2\text{-Mephen})^{2+}$	2.208	14
$Fe(MeIm)_6^{2+}$	2.197	15
$Fe[HB(Me_2pz)_3]_2$	2.172	11
$Fe(tppb)_2(SCN)(THF)$	2.132	12
$Fe(tacn)_2Cl_2$	2.034	16
$Fe(tri\text{-}2\text{-}pyridylamine)_2^{2+}$	1.982	17
$Fe[HB(pz)_3]_2$	1.973	11
$Fe(bpy)_3^{2+}$	1.966	18
$Fe(terpy)_2^{2+}$	1.955	19

(20) Cambridge Structural Database, Cambridge Crystallographic Data Centre, 1989.
(21) Raston, C. L.; White, A. H.; Golding, R. M. *J. Chem. Soc., Dalton Trans.* **1977**, 329.

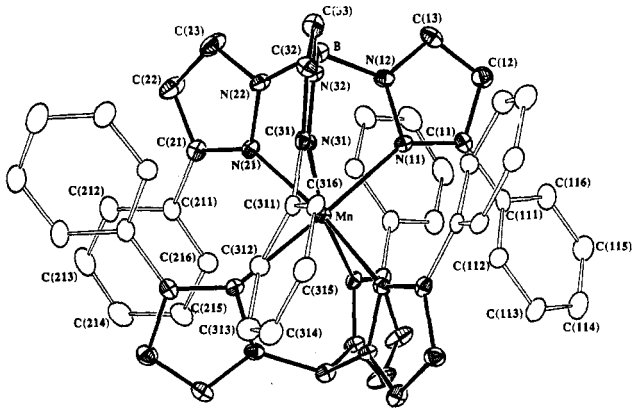

Figure 2. Solid-state structure of $Mn(tppb)_2$ (**2**) showing atom-labeling scheme. Hydrogen atoms are omitted for clarity.

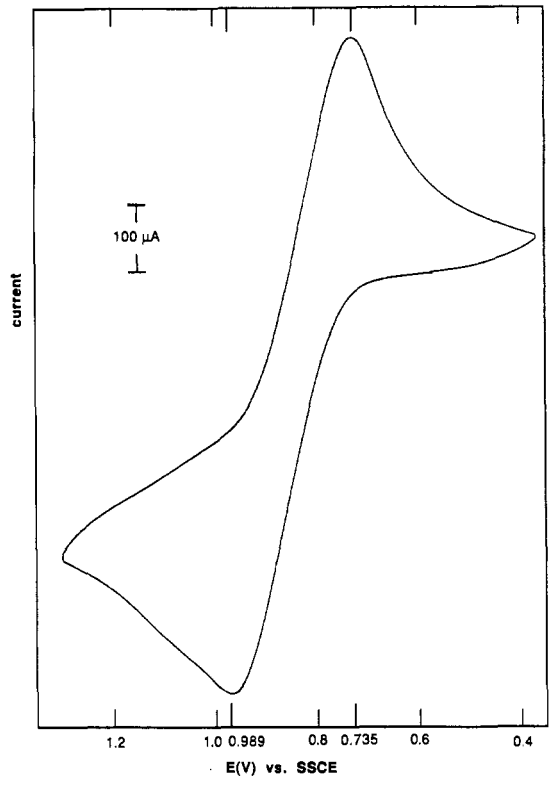

Figure 3. Cyclic voltammogram of $Fe(tppb)_2$ (**1**) recorded by using ca. 0.05 M Bu_4NPF_6 as supporting electrolyte, a Pt working electrode, an SSCE reference electrode, and a scan speed of 50 mV/s.

an octacoordinate naphthyridine species.[23] The long Fe–N bonds enable the iron atom to attain a high-spin configuration, which is unusual for Fe(II)–N_6 species. Although high-spin Fe–N bonds are generally longer than their low-spin counterparts, the bonds in $Fe(tppb)_2$ are still approximately 2% longer than the high-spin average.[24]

The structure and labeling scheme for $Mn(tppb)_2$ (**2**) are shown in Figure 2. The complex crystallizes as $\mathbf{2}\cdot 1.4CH_2Cl_2$ in the orthorhombic space group *Ibca* with the Mn atom situated on a crystallographic 2-fold axis relating the two ligands. Macroscopic features of the structure are similar to the iron analogue. The Mn–N bond lengths (average 2.32 Å) are relatively long for Mn(II)–nitrogen complexes, although they are not as anomalous as in the iron case. The average Mn(II)–N bond length in crystallographically characterized complexes (excluding Mn–N(nitrosyl) bonds) is 2.214 Å,[20] with values ranging from 1.909[25] to 2.517 Å for $Mn(bbt)(NCS)_2$.[26] Comparison can be made to the structure of $Mn^{II}[HB(3,5\text{-}Me_2pz)_3]_2$,[27] which has average Mn–N bond lengths of 2.275 Å, again demonstrating the steric requirements of the tppb ligand.

Electrochemistry

The effect of increasing the metal–nitrogen distances on the electronic properties of the iron center is demonstrated by the Fe^{III}/Fe^{II} reduction potential for **1**. The cyclic voltammogram for $Fe(tppb)_2$ (Figure 3) shows a quasi-reversible wave with $E_{1/2}$ = 0.855 V vs SSCE. Comparison with the less sterically encumbered $Fe[HB(pz)_3]_2$ shows that the Fe^{III}/Fe^{II} couple in the latter complex occurs at a much lower potential of 0.23 V vs SCE.[11] The ferric oxidation state is apparently destabilized by pulling the ligands away from the metal center. In fact, even though the (pyrazolyl)borate groups are negatively charged, the reduction potential for $Fe(tppb)_2$ is rather high for an Fe^{III}/Fe^{II} couple. As shown in Table VII, Fe^{III}/Fe^{II} couples have been observed over a wide range of potentials, but only a few, such as $Fe(phen)_3^{3+}$ and $Fe(Me_2bpy)_3^{3+}$, are more positive.

The cyclic voltammogram of $Mn(tppb)_2$ shows only irreversible waves at potentials approaching the solvent limits (±1.8 V vs SSCE). This contrasts greatly with the behavior of $Mn[HB(3,5\text{-}Me_2pz)_3]_2$, which displays a Mn^{III}/Mn^{II} reduction potential at ca. 0.02 V vs SSCE in CH_3CN solution.[27]

Magnetic Properties

Both of the metal complexes reported here show magnetic properties consistent with high-spin electronic configurations. After a diamagnetic correction for the ligand of $\chi_M = -5.732 \times 10^{-4}$ cm^3 mol^{-1} (determined experimentally for the potassium salt) is applied, the solid-state room-temperature magnetic susceptibilities are calculated as 5.12 μ_B for $Fe(tppb)_2$ (spin-only value for an $S = 2$ species is 4.90 μ_B) and 6.06 μ_B for $Mn(tppb)_2$ (expected 5.92 μ_B for an $S = {}^5/_2$ species). Furthermore, the ^1H NMR spectrum of $Fe(tppb)_2$ in $CDCl_3$ shows peaks ranging from 14.2 ppm upfield of TMS to 50.4 ppm downfield of TMS, characteristic of a species with organic ligands bound to a paramagnetic center. The magnetic data for the iron complex are interesting in that they follow a pattern evident in the less substituted analogues. While $Fe[HB(pz)_3]_2$ is low-spin at room

(22) Balch, A. L.; Chan, Y. W.; Olmstead, M. M.; Renner, M. W. *J. Org. Chem.* **1986**, *51*, 4651.
(23) Singh, P.; Clearfield, A.; Bernal, I. *J. Coord. Chem.* **1971**, *1*, 29.
(24) Butcher, R. J.; Addison, A. W. *Inorg. Chim. Acta* **1989**, *158*, 211.
(25) Cooper, D. J.; Ravenscroft, M. D.; Stotter, D. A.; Trotter, J. *J. Chem. Res.* **1979**, *287*, 3359.
(26) Takahashi, K.; Nishida, Y.; Kida, S. *Bull. Chem. Soc. Jpn.* **1984**, *57*, 2628.
(27) Chan, M. K.; Armstrong, W. H. To be submitted for publication.
(28) The following potentials (V) were used in making conversions to V vs NHE: Ag/Ag$^+$, 0.545; SCE, 0.242; SSCE, 0.236; Ag/AgCl, 0.222.
(29) Harris, W. R.; Carrano, C. J.; Cooper, S. R.; Sofen, S. R.; Avdeef, A. E.; McArdle, J. V.; Raymond, K. N. *J. Am. Chem. Soc.* **1979**, *101*, 6097.
(30) Latimer, W. M. *Oxidation Potentials*; Prentice Hall, Inc.: New York, 1938.
(31) Armstrong, W. H.; Spool, A.; Papaefthymiou, G. C.; Frankel, R. B.; Lippard, S. J. *J. Am. Chem. Soc.* **1984**, *106*, 3653.
(32) Nishida, Y.; Takeuchi, M.; Shimo, H.; Kida, S. *Inorg. Chim. Acta* **1984**, *96*, 115.
(33) Addison, A. W.; Wahlgreen, C. G. *Inorg. Chim. Acta* **1988**, *147*, 61.
(34) Kadish, K. M.; Morrison, M. M.; Constant, L. A.; Dickens, L.; Davis, D. G.; *J. Am. Chem. Soc.* **1976**, *98*, 8387.
(35) Kimura, E.; Kodama, M.; Machida, R.; Ishizu, K. *Inorg. Chem.* **1982**, *21*, 595.
(36) Dean, J. A., Ed. *Lange's Handbook of Chemistry*, 13th ed.; McGraw Hill Book Co.: New York, 1985.
(37) Wieghardt, K.; Schmidt, W.; Herrmann, W.; Küppers, H.-J. *Inorg. Chem.* **1983**, *22*, 2953.
(38) Donohoe, R. J.; Atamian, M.; Bocian, D. F. *J. Am. Chem. Soc.* **1987**, *109*, 5593.
(39) Wieghardt, K.; Tolksdorf, I.; Herrmann, W. *Inorg. Chem.* **1985**, *24*, 1230.
(40) (a) Gorton, J. E.; Lentzner, H. Z.; Watts, W. E. *Tetrahedron* **1971**, *27*, 4353. (b) Page, J. A.; Wilkinson, G. *J. Am. Chem. Soc.* **1952**, *74*, 6149.
(41) Powers, M. J.; Meyer, T. J. *J. Am. Chem. Soc.* **1978**, *100*, 4393.
(42) Weast, R. C., Astle, M. J., Eds. *CRC Handbook of Chemistry and Physics*, 63rd ed.; CRC Press Inc.: Boca Raton, FL, 1982.
(43) Garcia, E.; Kwak, J.; Bard, A. J. *Inorg. Chem.* **1988**, *27*, 4377.
(44) Serr, B. R.; Andersen, K. A.; Elliott, C. M.; Anderson, O. P. *Inorg. Chem.* **1988**, *27*, 4499.

Table VII. Reduction Potentials for Fe^{III}/Fe^{II} Couples

compd	pot., V	ref pot.	pot. vs NHE[28]	ref
Fe(enterobactin)	−1.23	SCE	−0.99	29
FeO_2^-	−0.68	NHE	−0.68	30
$Fe_2O[HB(pz)_3]_2(OAc)_2$	−0.76	SCE	−0.52	31
$Fe(Pctad)ClO_4$	−0.945	Ag/Ag^+	−0.400	33
$Fe(Saltad)ClO_4$	−0.79	Ag/Ag^+	−0.25	33
Fe(Mesaldpt)Cl	−0.66	Ag/Ag^+	−0.12	33
Fe(TPP)Cl	−0.29	SCE	−0.05	34
Fe(py-pentaamine)$^{2+}$	−0.27	SCE	−0.03	35
$Fe(EDTA)^-$	0.12	NHE	0.12	36
$Fe([16]aneN_5)$	−0.04	SCE	0.20	36
$Fe(ibz)Cl_3$	−0.4	Fc^+/Fc	0.30	32
$Fe[(TPP)Br_4]$	0.083	Ag/AgCl	0.305	38
$Fe(tacn)_2$	0.13	Ag/AgCl	0.35	37
$Fe[TPP(CN)_3]$	0.185	Ag/AgCl	0.407	38
$Fe(dtne)Br_3$	0.41	NHE	0.41	39
$Fe[TPP(CN)_4]$	0.215	Ag/AgCl	0.438	38
$Fe[HB(pz)_3]_2^+$	0.23	SCE	0.47	31
$Fe(CN)_6^{3-}$	0.55	NHE	0.55	36
Fc^+	0.34	SCE	0.58	40
Fc—C≡C—Fc	0.46, 0.60	SSCE	0.70, 0.84	41
$Fe^{3+}(aq)$	0.77	NHE	0.77	42
$Fe(bpy)_3^{3+}$	0.82	SCE	1.06	43
$Fe(tppb)_2$	0.855	SSCE	1.091	this work
$Fe(phen)_3^{3+}$	1.14	NHE	1.14	30
$Fe(Me_2bpy)_3^{3+}$	0.912	SCE	1.154	44
$Fe(NO_2phen)_3^{3+}$	1.25	NHE	1.25	30

temperature and undergoes a spin crossover at 393 K, $Fe[HB(3,5\text{-}Me_2pz)_3]_2$, with longer Fe–N bond lengths, was found to be high-spin at room temperature.[11] Thus, it is not surprising that $Fe(tppb)_2$, with still longer Fe–N bonds, is a high-spin complex at room temperature. Similar conversion of a spin-crossover Fe(II) system to a high-spin Fe(II) complex has been observed previously.[45]

Conclusions

Despite expectations to the contrary, a phenyl group substituent in the 3-position of the pyrazole ring in the hydrotris(pyrazol-1-yl)borate ligand is not sufficiently bulky to prevent formation of the bis complex in the absence of a strongly coordinating ligand such as SCN^-. In the context of non-heme oxygenase modeling this is disappointing, as one would prefer to maintain open coordination sites for binding of substrate and/or dioxygen. On the other hand, we have observed a greater reactivity of **1** and **2** toward O atom donors such as PhIO and MCPBA as compared to their less hindered counterparts, presumably indicating that removal of one of the bulky ligands is feasible. This is not surprising on the basis of the marked increase in Fe–N bond lengths for **1** compared to $Fe(HBpz_3)_2$. In addition to providing a more reactive metal center, the bulky ligand causes large shifts in the redox potentials for both Fe^{III}/Fe^{II} and Mn^{III}/Mn^{II} couples. Further investigations into the reactivities of **1** and **2**, particularly under oxidizing conditions, are underway.

Acknowledgment. Support for this work was provided by Grant No. GM382751-01 from the National Institutes of General Medical Sciences. We thank Dr. Frederick J. Hollander and Dr. Marilyn M. Olmstead for assistance with the crystal structure determinations.

Registry No. **1**, 128576-17-0; **2**, 128576-18-1; Ktppb, 106209-98-7; $Fe[HB(pz)_3]_2^+$, 86549-95-3; KBH_4, 13762-51-1; 3-phenylpyrazole, 2458-26-6.

Supplementary Material Available: For both **1** and **2**, tables of positional and isotropic equivalent thermal parameters, anisotropic thermal parameters, intramolecular distances, and intramolecular angles (21 pages); listings of structure factors for **1** and **2** (57 pages). Ordering information is given on any current masthead page.

(45) Harris, C. R.; Patil, H. R. H.; Sinn, E. *Inorg. Chem.* **1969**, *8*, 101.

Notes

Contribution from the Department of Chemistry, University of Wyoming, Laramie, Wyoming 82071

Calcium Binding to Carboxylate Residues: Synthesis and Structure of a New Form of Calcium Malonate

Derek J. Hodgson* and R. Owen Asplund

Received February 14, 1990

There has been intense recent interest in the modes of binding of the calcium ion to carboxylate and (especially) dicarboxylate moieties because of the significance of such interactions in the blood and bone proteins that contain the modified amino acid residues γ-carboxyglutamic acid (Gla) and β-carboxyaspartic acid (Asa).[1-5] It is well established that Gla residues are implicated in the binding of calcium ions in both blood and bone proteins,[6] and several authors have suggested that a principal role for Gla might be in the discrimination between calcium and magnesium ions.[7] Consequently, we and others have been investigating the structural properties of a series of model complexes that are designed to permit the evaluation of the possible modes of binding of calcium, magnesium, and related metals to Gla and/or Asa.[8-11]

The binding of calcium ions to carboxylates has been discussed exhaustively by Einspahr and Bugg;[12] these authors note that a monocarboxylate (e.g. Glu or Asp) can bind to calcium in either of two ways. In a unidentate mode (**1**) the metal binds to a single oxygen atom, while in a bidentate fashion (**2**) the metal binds to

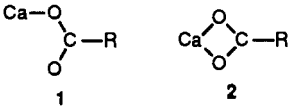

1 **2**

both oxygen atoms of the carboxylate group. In a dicarboxylate (e.g. Gla or Asa) there is an additional possible mode in which the metal ion binds to two oxygen atoms from different carboxylate groups; this mode of binding, which is sometimes referred to as the "malonate" mode since it is uniquely available to a dicarboxylate like malonate, is shown in **3**.

(1) Magnusson, S.; Sottrup-Jensen, L.; Peterson, T. E.; Morris, H. R.; Dell, A. *FEBS Lett.* **1974**, *44*, 189-193.
(2) Stenflo, J.; Fernlund, P.; Egan, W.; Roepstorff, P. *Proc. Natl. Acad. Sci. U.S.A.* **1974**, *71*, 2730-2733.
(3) Prendergast, F. G.; Mann, K. G. *J. Biol. Chem.* **1977**, *252*, 840-850.
(4) Lian, J. B.; Hauschka, P. V.; Gallop, P. M. *Fed. Proc.* **1978**, *37*, 2615-2620.
(5) Christy, M. R.; Barkley, R. M.; Koch, T. H.; Van Buskirk, J. J.; Kirsch, W. M. *J. Am. Chem. Soc.* **1981**, *103*, 3935-3937; Christy, M. R.; Koch, T. H. *J. Am. Chem. Soc.* **1982**, *104*, 1771-1772.
(6) Jackson, C. M.; Nemerson, Y. *Annu. Rev. Biochem.* **1980**, *49*, 765-811.
(7) Williams, R. J. In *Calcium Binding Proteins and Calcium Function*; Wasserman, R. H., et al., Eds.; Elsevier: New York, 1977; pp 1-12.
(8) Zell, A.; Einspahr, H.; Bugg, C. E. *Biochemistry* **1985**, *24*, 533-537.
(9) Curry, M. E.; Eggleston, D. S.; Hodgson, D. J. *J. Am. Chem. Soc.* **1985**, *107*, 8234-8238. Curry, M. E.; Hodgson, D. J.; Eggleston, D. S. *Rev. Port. Quim.* **1985**, *27*, 344.
(10) Yokomori, Y.; Hodgson, D. J. *Inorg. Chem.* **1988**, *27*, 2008-2011.
(11) Yokomori, Y.; Flaherty, K. A.; Hodgson, D. J. *Inorg. Chem.* **1988**, *27*, 2300-2306.
(12) Einspahr, H.; Bugg, C. E. *Acta Crystallogr., Sect. B* **1981**, *B37*, 1044-1052.

0020-1669/90/1329-3612$02.50/0